ACS OMEGA

http://pubs.acs.org/journal/acsodf

Article

Adsorption of 5-Hydroxymethylfurfural, Levulinic Acid, Formic Acid, and Glucose Using Polymeric Resins Modified with Different Functional Groups

Lei Hu,[‖] Jiayi Zheng,[‖] Qing Li, Shunhui Tao, Xiaojie Zheng, Xiaodong Zhang, Yao Liu, and Xiaoqing Lin*

Cite This: *ACS Omega* 2021, 6, 16955−16968

Read Online

ACCESS | Metrics & More | Article Recommendations | Supporting Information

ABSTRACT: 5-hydroxymethylfurfural (5-HMF) is a promising high value-added platform chemical, which can be produced from glucose, fructose, or lignocellulosic biomass via catalysis technology. However, the effective separation of 5-HMF from aqueous solution and actual biomass hydrolysate is still challenging because 5-HMF can be further rehydrated into levulinic acid (LA) and formic acid (FA) under acidic conditions. Herein, the adsorption behavior of glucose and 5-HMF and its follow-up products (LA and FA) from aqueous solutions onto polymeric adsorbents modified with various functional groups (XAD-4, XAD7HP, and XAD761 resins) was systematically investigated. The results showed that XAD761 resin exhibited the highest adsorption selectivity ($\alpha_{5\text{-HMF/glucose}}$ = 42.42 ± 5.84, $\alpha_{5\text{-HMF/FA}}$ = 18.41 ± 0.50, and $\alpha_{5\text{-HMF/LA}}$ = 3.01 ± 0.10) and capacity for 5-HMF (106 mg g^{-1} wet resin). The adsorption equilibrium was better fitted by the Freundlich isotherm model at the studied range of 5-HMF concentrations. The thermodynamic study and activation energy also revealed that the adsorption process of XAD761 resin for 5-HMF was spontaneous, exothermic, and physical. The kinetic regression results revealed that the kinetic data of 5-HMF was accurately followed by the pseudo-second-order kinetic model. In conclusion, the present study revealed that the potential of phenol formaldehyde resin with hydroxyl groups could be used as an adsorbent for aldehyde organic compounds.

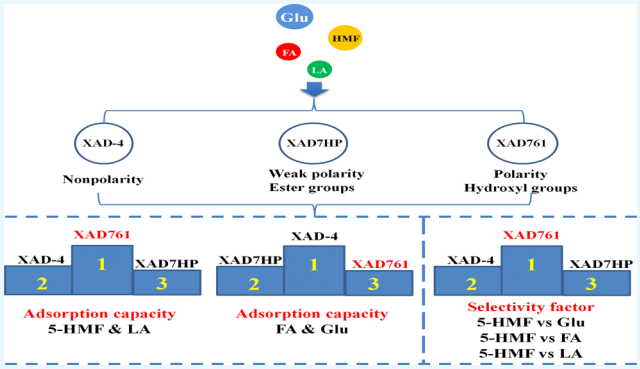

1. INTRODUCTION

Petroleum, coal, and natural gas industries have made significant contributions to mankind and played a vital role in the sustainable development of economy and society.[1,2] However, owing to the declining supply and rising cost of fossil resources, combined with the global warming and climate change, great attention has been paid on sustainable routes to produce chemicals, solvents, and fuels from renewable lignocellulosic biomass.[3,4] Lignocellulosic biomass, as the maximum renewable plant biomass in nature, can be transformed into high value-added platform chemicals by chemical catalysis technology or biorefinery.[5,6] Among these attractive platform chemicals, 5-hydroxymethylfurfural (5-HMF) has drawn increasing interest as a potential biomass-derived platform chemical, which can be produced from C6 sugars (i.e., glucose and fructose) via acid catalysts.[7−14] Furthermore, 5-HMF can be used as a building block platform to synthesis high value-added chemicals currently being produced from fossil resources, such as levulinic acid (LA), 2,5-dimethylfuran, 2,5-furandicarboxylic acid, and 2,5-diformylfuran.[15−21] LA is one of United States Department of Energy's top 12 platform chemicals because it can be used as spice raw materials, pesticide intermediates, animal feed, resin raw materials, coatings, and so forth.[22] Formic acid (FA) is a biomass-derived organic acid, and it can be used in leather, dye, medicine, and rubber industries for its low cost and abundant supply.[23]

However, 5-HMF can be further rehydrated into byproducts under acidic conditions, such as LA, FA, and humins,[24,25] which results in great difficulty to separate and purify 5-HMF from such diluted and complex multicomponent systems.[26] In the last two decades, considerable efforts have been devoted to the selection and optimization of the catalyst systems to enhance C6 sugar conversion as well as 5-HMF yields.[27−29] However, only a few investigations have been focusing on the separation of 5-HMF from such dilute aqueous solutions or

Received: April 9, 2021
Accepted: June 16, 2021
Published: June 24, 2021

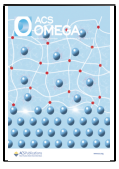

ACS Publications

© 2021 The Authors. Published by American Chemical Society

https://doi.org/10.1021/acsomega.1c01894
ACS Omega 2021, 6, 16955−16968

hydrolysates.[30−39] Separation and recovery of 5-HMF by distillation not only requires high energy consumption but also leads to a great risk of polymerization of 5-HMF due to instability at high temperature. Vinke and Bekkum[30] first presented selectively recovered 5-HMF from aqueous mixtures with fructose and LA using three activated carbons in terms of R0.8 A, ROX 0.8, and C-granular. Ranjan et al.[31] proposed using three different surface-modified activated carbons to selectively adsorb 5-HMF from fructose/DMSO mixtures. The results show that the microporosity and oxygen-containing functional groups of adsorbent are very important for the adsorption capacity and selectivity of 5-HMF. León et al.[34] investigated the adsorption of 5-HMF from fructose hydrolysate using H-BEA zeolite with SiO_2/Al_2O_3 = 18 and found that the zeolite H-BEA showed stronger capacity to 5-HMF and LA than sugars and FA from aqueous solution. Although these nonpolar porous materials possess high 5-HMF adsorption capacity owing to their high surface area, the adsorption selectivity and desorption rate remain low.[40] It raises a question whether a new adsorbent material can improve the adsorption performance in terms of high adsorption capacity, high selectivity, high desorption rate, and fast diffusion rate (3-H−1-F).[41]

Compared to activated carbons and zeolite, hyper-cross-linked polymer (HCP) possesses advantages in terms of large specific surface area, rigid skeleton structure, easy regeneration, and stable physical and chemical properties, which have attracted extensive attention in separation,[41−44] gas storage,[45−47] and heterogeneous catalysis.[48] Rose et al.[32] developed a HCP to recover 5-HMF from aqueous solution. It was concluded that the adsorption selectivity of 5-HMF depended on the specific surface area, the pore volume, and the surface polarity of the HCP. In our previous study, the adsorption behavior of 5-HMF onto an amide functional group-modified HCP from both single-component and multicomponent systems was systematically investigated.[33] The result shows that the hydrophobic interaction between the benzene ring skeleton and the furan ring of 5-HMF and the hydrogen bond between the functional amide groups of SY-01 resin particle and the aldehyde functional group of 5-HMF played a key role in the adsorption process.[33]

To further evaluate the feasibility of the adsorbent, which can form hydrogen bond force with 5-HMF, could be used for the separation and purification of 5-HMF. In the current work, three different commercial porous resins (XAD-4 without functional group, XAD7HP with ester functional group, and XAD761 with hydroxyl functional group) were used to adsorb 5-HMF, LA, FA, and glucose in single-component and multicomponent systems. Furthermore, the equilibrium isotherm, kinetic simulation, and thermodynamics were systematically investigated.

2. MATERIALS AND METHODS

2.1. Materials. Analytical grade (AR) glucose (Glu, 99.0%), FA (99.0%), and LA (99.0%) were obtained from Shanghai Aladdin Bio-Chem Technology Co., Ltd. (Shanghai, China). 5-HMF (AR, ≥98%) was purchased from Nanjing Spring & Autumn Biological Engineering Co., Ltd. Details of the chemicals are given in Table 1. Amberlite resins (XAD-4, XAD7HP, and XAD761) were purchased from Rohm & Hass. The physical characteristics of these three resins are listed in Table 2. All chemicals used in this study were never further purified.

Table 1. CAS Registry Number, Suppliers, and Mass Fraction of the Chemicals

component	CAS reg. no.	suppliers	mass fraction
glucose	14431-43-7	Shanghai Aladdin Bio-Chem Technology Co., Ltd.	0.990
FA	64-18-6	Shanghai Aladdin Bio-Chem Technology Co., Ltd.	0.990
LA	123-76-2	Shanghai Aladdin Bio-Chem Technology Co., Ltd.	0.990
5-HMF	67-47-0	Nanjing Spring & Autumn Biological Engineering Co., Ltd.	≥0.980

Table 2. Physical Properties of the XAD-4, XAD7HP, and XAD761 Resins

resin	XAD-4	XAD7HP	XAD761
surface area ($m^2\ g^{-1}$)	750	500	200
particle size (μm)	640	560	700
average pore diameter (nm)	100	450	600
polarity	nonpolarity	weak polarity	polarity
functional groups		ester groups	hydroxyl groups

2.2. Methods. *2.2.1. Selectivity Factor Testing.* XAD-4, XAD7HP, and XAD761 resins were used to test the selectivity factor in the mixture containing 5-HMF, LA, FA, and glucose using batch experiments. Typically, 1.0 g of wet resin was weighed by an electronic balance (CP224C, Changzhou Ohaus Instrument Co., Ltd., Changzhou, China) after vacuum filtration (SHZ-DIII, Gongyi Yuhua Instrument Co., Ltd., Gongyi, China) and added to 50 mL of 5-HMF-LA-FA-Glu mixture solution (5-HMF: 5.021 g L^{-1}, LA: 20.251 g L^{-1}, FA: 9.103 g L^{-1}, and glucose: 9.854 g L^{-1}) in a 100 mL conical flask and maintained at 298 K for 4 h with the speed of 120 rpm in a constant temperature incubator shaker (ZQZY-80BS, Shanghai Zhichu Instrument Co., Ltd., Shanghai, China). After reaching the equilibrium state, the concentrations of the adsorbate were determined by high-performance liquid chromatography (HPLC, Agilent Technologies 1200 Series, USA). The experiments were carried out three times, and the mean values were recorded for evaluation. The capacity of the adsorbate and the selectivity of 5-HMF to LA, FA, and glucose were calculated by the following equations[42,49]

$$q_{i,e} = \frac{(C_{i,0} - C_{i,e}) \times V}{m} \quad (1)$$

$$\alpha_i^{5\text{-HMF}} = \frac{q_{5\text{-HMF,e}} \cdot C_{i,e}}{q_{i,e} \cdot C_{5\text{-HMF,e}}} \quad (2)$$

2.2.2. Adsorption Equilibrium Experiments. Batch adsorption equilibrium experiments were conducted in a shaking incubator (ZQZY-80BS, Shanghai Zhichu Instrument Co., Ltd., Shanghai, China) with temperature control and reciprocating shaking. The tests of saturated adsorption behavior of three different resins (XAD-4, XAD7HP, and XAD761) were carried out using glucose, 5-HMF, FA, and LA at 288, 298, 308, and 318 K accompanied by different initial concentrations in the single-component system. The detailed operation process is the same as that described in Section 2.2.1. Adsorption experiments were repeated three times, and the average value was used for evaluation. The experimental

https://doi.org/10.1021/acsomega.1c01894
ACS Omega 2021, 6, 16955−16968

equilibrium adsorption capacity, q_e (mg g^{-1}), was calculated according to eq 1.

2.2.3. Adsorption Kinetic Studies. The batch adsorption kinetic experiments were performed in three-necked bottles with a thermometer and stirrer to investigate the effect of temperature on 5-HMF adsorption onto XAD761 resin. Briefly, 10.0 g of XAD761 wet resin was added to the flask containing 500 mL of a certain initial 5-HMF concentration in a collector-type constant temperature heating magnetic stirrer (DF-101S, Gongyi Yuhua Instrument Co., Ltd., Gongyi, China) at 288, 298, 308, and 318 K. The 5-HMF solution with XAD 761 resin was shaken by an IKA cantilever agitator (RW 20 digital, Aika (Guangzhou) instrument equipment Co., Ltd., Guangzhou, China) at the speed of 120 rpm. All adsorption kinetic studies were carried out three times. The samples were collected at preset time intervals, filtered, and detected by HPLC. The amount at any time, q_t (mg g^{-1}), was calculated by eq 3.

$$q_t = \frac{(C_0 - C_t) \times V}{m} \tag{3}$$

2.2.4. Analysis Method. The concentrations of glucose, FA, LA, and 5-HMF were determined by an Agilent 1200 HPLC instrument equipped with a hydrogen-form Aminex HPX-87H anion exchange column (300 mm × 7.8 mm, Bio-Rad Corp., CA, USA). The separation conditions were set as follows:[33,43] flow rate: 0.5 mL min^{-1}, mobile phase: 5 mM sulfuric acid, sample injection volume: 20 μL, detector: refractive index detector (RID, Agilent Technologies 1260 Infinity II) and UV, column temperature: 65 °C, and RID detector temperature: 55 °C.

3. RESULTS AND DISCUSSION

3.1. Adsorption Equilibrium Selectivity Factor. To evaluate the differences in affinity between the adsorbate (glucose, FA, LA, and 5-HMF) and different functional modified resins (XAD-4, XAD7HP, and XAD761), competitive adsorption experiments were performed toward coexisting multicomponent solution (5.021 g L^{-1} 5-HMF, 20.251 g L^{-1} LA, 9.103 g L^{-1} FA, and 9.854 g L^{-1} glucose). Figure 1 (data given in Tables S1 and S2) represents the equilibrium capacities of glucose, FA, LA, and 5-HMF onto various resins and selectivity factors of $\alpha_{5\text{-HMF/glucose}}$, $\alpha_{5\text{-HMF/FA}}$, and $\alpha_{5\text{-HMF/LA}}$. As illustrated in Figure 1, all three different functional modified resins displayed much higher adsorption capacity toward 5-HMF and LA than toward FA and glucose. It is worth noting that the 5-HMF and LA capacities onto XAD761 resin were higher than the other two resins. Most importantly, the selectivity factors $\alpha_{5\text{-HMF/glucose}}$, $\alpha_{5\text{-HMF/FA}}$, and $\alpha_{5\text{-HMF/LA}}$ onto XAD761 resin reached up to 42.42 ± 5.84, 18.41 ± 0.50, and 3.01 ± 0.10, respectively, suggesting that 5-HMF and LA molecules could specifically bind to the active adsorption sites on XAD761 resin. While glucose and FA have no special recognition sites, they are difficult to be adsorbed on XAD-761 resin and transferred straightforwardly through XAD761 with low resistance. Furthermore, the selectivity factors $\alpha_{5\text{-HMF/glucose}}$ (42.42 ± 5.84), $\alpha_{5\text{-HMF/FA}}$ (18.41 ± 0.50), and $\alpha_{5\text{-HMF/LA}}$ (3.01 ± 0.10) were much higher than XAD-4 and XAD7HP resins, which further demonstrated that the XAD761 resin had higher recognition specificity to 5-HMF and easily separates 5-HMF from multicomponent mixture solution. This may be because the 5-HMF molecule contains aldehyde and hydroxyl groups

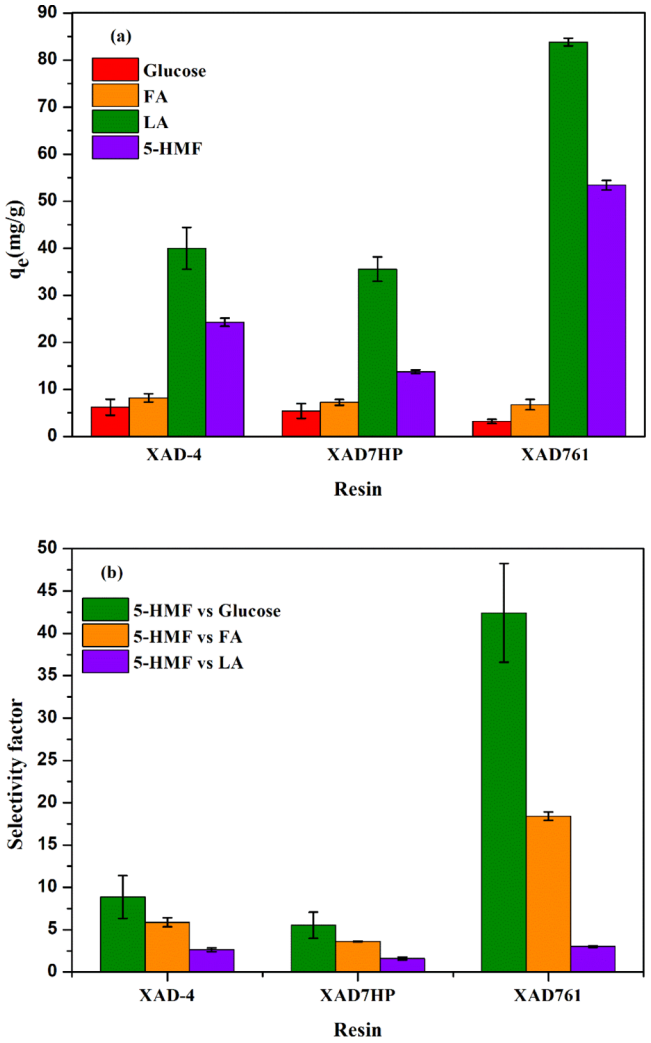

Figure 1. Adsorption capacity (a) and selectivity (b) of 5-HMF (5.021 g L^{-1}), LA (20.251 g L^{-1}), FA (9.103 g L^{-1}), and glucose (9.854 g L^{-1}) onto XAD-4, XAD7HP, and XAD761 resins in a multicomponent system at 298 ± 1 K.

and can combine with XAD761 resin through hydrogen bonding interaction, as well as hydrophobic interaction between the benzene ring of phenol formaldehyde resin and the furan ring of 5-HMF.[33,50]

3.2. Adsorption Isotherms. It is important to describe the interaction between the adsorbate and surface properties of the adsorbent by various equilibrium adsorption isotherm model analyses.[51,52] In this work, the equilibrium adsorption data of 5-HMF, LA, FA, and glucose were determined using three adsorbents with different functional groups (XAD-4, XAD7HP, and XAD761) in a single-component solution system. Four temperatures of 288, 298, 308, and 318 K were chosen for the investigation of adsorption isotherms. Langmuir,[53] Freundlich,[54] and Henry isotherm[55] models were applied to fit the experimental equilibrium adsorption data.

$$\text{Langmuir isotherm model } q_e = \frac{q_m K_L C_e}{1 + K_L C_e} \tag{4}$$

$$\text{Freundlich isotherm model } q_e = K_F C_e^{1/n} \tag{5}$$

$$\text{Henry isotherm model } q_e = K_H C_e \tag{6}$$

https://doi.org/10.1021/acsomega.1c01894
ACS Omega 2021, 6, 16955−16968

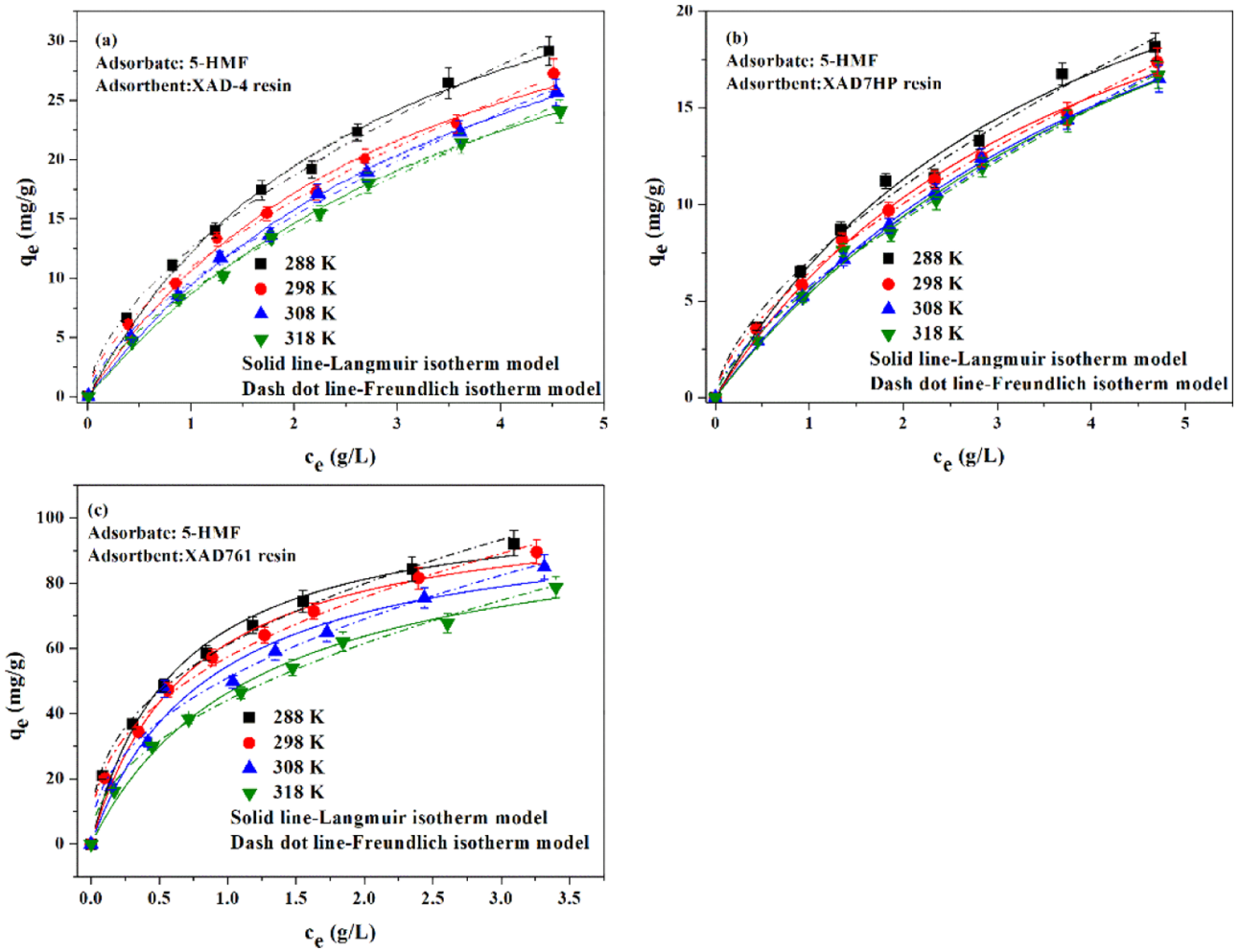

Figure 2. Adsorption of 5-HMF onto XAD-4 (a), XAD7HP (b), and XAD761 (c) resins in a single-component system at 288, 298, 308, and 318 K.

Table 3. Isotherm Parameters of Each Isotherm Model for the Adsorption of 5-HMF Onto Three Resins (XAD-4, XAD7HP, and XAD761) at 288−318 K

		Langmuir				Freundlich		
resin	T (K)	q_m (mg/g)	K_L (L/g)	R^2	R_L	K_F (mg/(g·(L/g)$^{1/n}$))	$1/n$	R^2
XAD-4	288	47	0.349	0.9897	0.36−0.85	12.547	0.579	0.9953
	298	45	0.312	0.9837	0.39−0.86	10.980	0.598	0.9956
	308	49	0.241	0.9952	0.45−0.89	9.762	0.650	0.9952
	318	48	0.221	0.9959	0.47−0.90	8.998	0.665	0.9952
XAD7HP	288	33	0.265	0.9823	0.43−0.88	7.086	0.626	0.9829
	298	31	0.247	0.9915	0.44−0.89	6.461	0.637	0.9965
	308	35	0.188	0.9992	0.51−0.91	5.769	0.693	0.9943
	318	37	0.173	0.9925	0.53−0.92	5.642	0.703	0.9951
XAD761	288	106	1.634	0.9707	0.11−0.55	61.086	0.386	0.9928
	298	105	1.415	0.9758	0.12−0.58	57.332	0.401	0.9892
	308	102	1.159	0.9494	0.15−0.63	50.931	0.438	0.9601
	318	102	0.837	0.9831	0.19−0.70	44.143	0.479	0.9915

The equilibrium adsorption isotherms of 5-HMF with various initial concentrations onto XAD-4, XAD7HP, and XAD761 resins were carried out at the studied temperatures and are shown in Figure 2 (data given in Tables S3−S5). The corresponding isotherm parameters obtained from nonlinear regression of experimental data are shown in Table 3. It can be observed from Figure 2 that the 5-HMF equilibrium adsorption capacities onto the three resins were negatively correlated with temperature. At the same temperature, the adsorption capacity of 5-HMF on the three resins increased with the increase of initial concentration and then gradually tended to equilibrium. Furthermore, as seen from Table 3, the parameters of K_L decreased with increasing temperature, indicating the fact that higher adsorption capacity can result from the large BET surface and pore volume.[55] During the experimental concentration range, the adsorption of 5-HMF on the three resins was favorable ($0 < R_L = 1/1 + K_L C_0 < 1$, $0 < 1/n < 1$).[51,56,57] The regression correlation coefficients of the

https://doi.org/10.1021/acsomega.1c01894
ACS Omega 2021, 6, 16955−16968

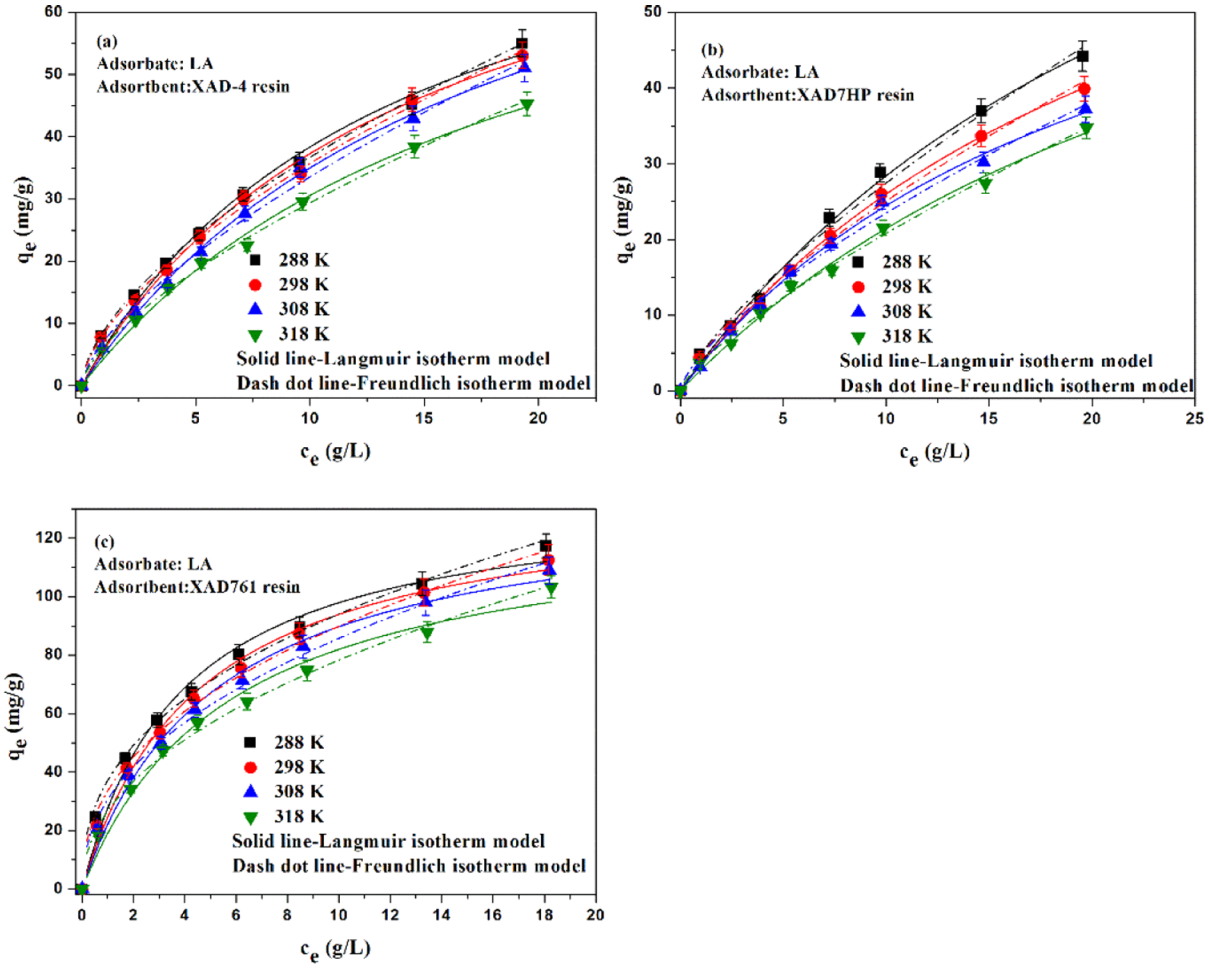

Figure 3. Adsorption of LA onto XAD-4 (a), XAD7HP (b), and XAD761 (c) resins in a single-component system at 288, 298, 308, and 318 K.

Table 4. Isotherm Parameters of Each Isotherm Model for the Adsorption of LA onto Three Resins (XAD-4, XAD7HP, and XAD761)

		Langmuir				Freundlich		
resin	T (K)	q_m (mg/g)	K_L (L/g)	R^2	R_L	K_F (mg/g·(L/g)$^{1/n}$)	$1/n$	R^2
XAD-4	288	91	0.072	0.9892	0.40−0.93	8.946	0.613	0.9987
	298	92	0.068	0.9899	0.42−0.93	8.481	0.624	0.9966
	308	97	0.056	0.9866	0.47−0.95	7.245	0.666	0.9929
	318	88	0.053	0.9923	0.48−0.95	6.305	0.668	0.9967
XAD7HP	288	109	0.035	0.9945	0.58−0.97	4.890	0.750	0.9904
	298	91	0.040	0.9968	0.55−0.96	4.709	0.726	0.9934
	308	76	0.047	0.9967	0.51−0.95	4.661	0.702	0.9904
	318	86	0.033	0.9931	0.60−0.97	3.680	0.752	0.9951
XAD761	288	136	0.256	0.9718	0.16−0.79	37.221	0.403	0.9944
	298	136	0.221	0.9858	0.18−0.82	33.664	0.427	0.9891
	308	135	0.196	0.9856	0.20−0.83	30.723	0.446	0.9922
	318	129	0.175	0.9801	0.22−0.85	26.747	0.467	0.9929

Freundlich isotherm model were better than those of the Langmuir isotherm model, suggesting that the adsorption of 5-HMF onto the surface of XAD761 resin was heterogeneous. The values of K_F were decreased with increasing temperature, indicating the exothermic nature of the adsorption process.[58] Moreover, it is worth noting that the uptakes of 5-HMF onto XAD761 resin were all higher than those onto XAD-4 and XAD7HP resins at all studied temperatures and initial concentrations. The highest uptake of 5-HMF was 106 mg g^{-1} wet resin in the experimental concentration range (0.51−5.06 g L^{-1}) at 288 K. The main reason is that 5-HMF can be adsorbed onto resins through hydrogen bonding between the phenolic hydroxyl of the XAD761 resin and the aldehyde group of 5-HMF, as well as $\pi-\pi$ stacking generated between the benzene ring of the XAD761 resin and the furan ring of 5-HMF.[33] The hydrophobic−hydrophobic forces and hydrogen bond forces copromote the adsorption capacity of 5-HMF.

https://doi.org/10.1021/acsomega.1c01894
ACS Omega 2021, 6, 16955−16968

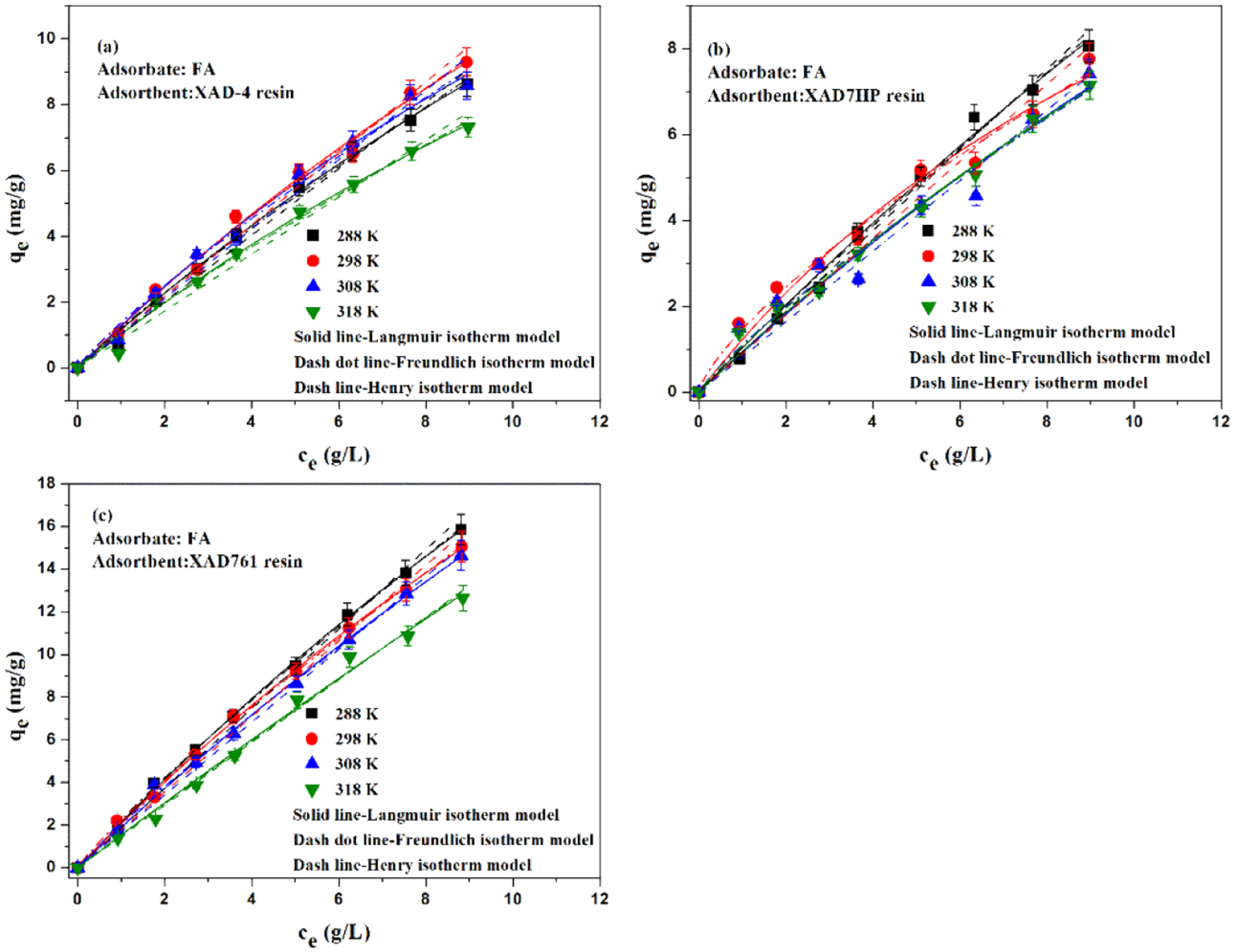

Figure 4. Adsorption of FA onto XAD-4 (a), XAD7HP (b), and XAD761 (c) resins in a single-component system at 288, 298, 308, and 318 K.

Furthermore, the equilibrium adsorption of LA onto the three resins is displayed in Figure 3 (data given in Tables S6–S8), and the model parameters are listed in Table 4. It can be concluded that the equilibrium data of LA at different adsorption temperatures could also be better described by the Freundlich model, and the variations of the model parameters of LA onto the three kinds of resins are similar to those of 5-HMF. The adsorption capacity of LA onto XAD761 resin is higher than those onto XAD-4 and XAD7HP. The main reason is due to the fact that the phenolic hydroxyl group of the XAD761 resin can form a hydrogen bond with the carboxyl group of LA, and the n-alkyl group of LA forms $\pi-\pi$ hydrophobic force with the benzene ring of the resin.[42]

In addition, the adsorption experiments of FA and glucose were also studied, the results are displayed in Figures 4 and 5 (data given in Tables S9–S14), and the isotherm constants are listed in Tables 5 and 6, respectively. Clearly, the adsorption isotherms of FA and glucose are in a straight line which is typical of low surface coverage and poor affinity between the adsorbate and adsorbents, especially when the isotherm is represented by Henry's law.[55] In the process of liquid-phase adsorption, the capacity of the adsorbate depends not only on the affinity between the adsorbate and the adsorbent but also on the interaction between the adsorbate and the solvent, as well as the affinity between the solvent and the adsorbent.[59] The skeleton of the three resins is hydrophobic, while FA and glucose are hydrophilic and water-soluble substances, increasing their preference for remaining in the aqueous phase rather than being adsorbed. Thus, FA and glucose present a lower affinity for adsorption on the resins. It can be seen from Tables 5 and 6 that during the experimental concentration range, both R_L and $1/n$ values of FA were very close to 1, while all R_L values of glucose were equal to 1 and all $1/n$ values of glucose were greater than 1, indicating that FA and glucose are weak adsorption components. The comparison of the three adsorption models shows that the equilibrium data of FA and glucose are better fitted by the Henry isotherm model. All K_H values obtained from the Henry isotherm model at different temperatures decreased with increasing temperature, implying that the adsorption capacity of FA and glucose decreases gradually with the increase of adsorption temperature.

As can be seen from Table 3, the highest adsorption uptake of 5-HMF onto XAD761 resin was 106 mg g^{-1} wet resin in the experimental concentration range (0.51–5.06 g L^{-1}) at 288 K. At present, some researchers have studied the adsorption capacities of several adsorption resins for 5-HMF in different-component solution. By comparing the results obtained in this study with those in previously published reports (Table 7) on various adsorption resins in different-component solution for 5-HMF, it can be concluded that our findings are extremely good. This information may be useful for further research and

https://doi.org/10.1021/acsomega.1c01894
ACS Omega 2021, 6, 16955−16968

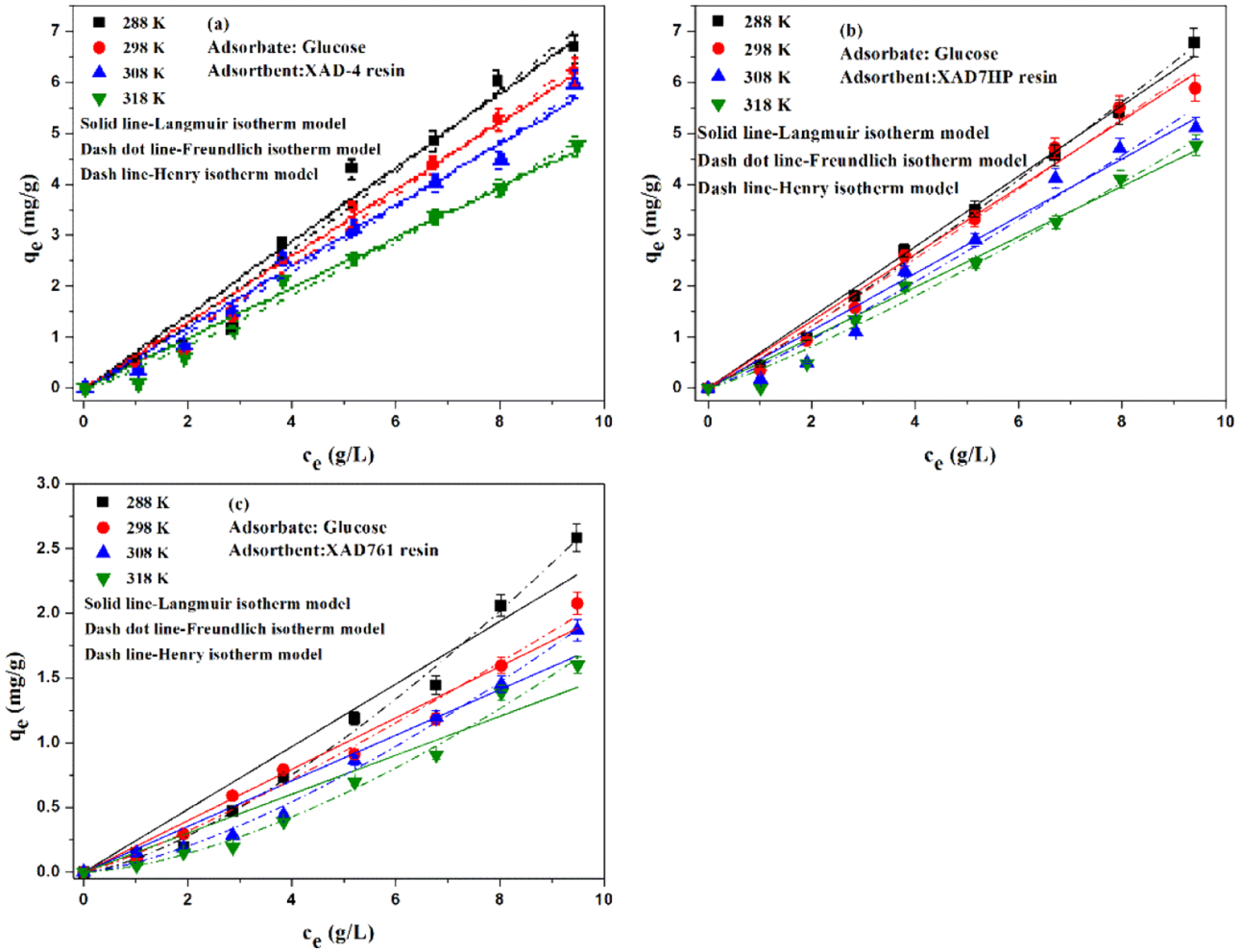

Figure 5. Adsorption of glucose onto XAD-4 (a), XAD7HP (b), and XAD761 (c) resins in a single-component system at 288, 298, 308, and 318 K.

Table 5. Isotherm Parameters of Each Isotherm Model for the Adsorption of FA onto Three Resins (XAD-4, XAD7HP, and XAD761)

		Langmuir				Freundlich			Henry	
resin	T (K)	q_m (mg/g)	K_L (L/g)	R^2	R_L	K_F (mg/g·(L/g)$^{1/n}$)	$1/n$	R^2	K_H (L/kg)	R^2
XAD-4	288	45	0.0264	0.9959	0.81−0.98	1.224	0.899	0.9931	1.010	0.9986
	298	47	0.0277	0.9897	0.80−0.97	1.359	0.882	0.9889	1.087	0.9954
	308	35	0.0382	0.9887	0.74−0.96	1.384	0.857	0.9841	1.055	0.9932
	318	34	0.0307	0.9896	0.78−0.97	1.079	0.884	0.9861	0.865	0.9947
XAD7HP	288	64	0.0164	0.9911	0.87−0.98	1.051	0.942	0.9891	0.942	0.9969
	298	20	0.0669	0.9663	0.62−0.94	1.468	0.739	0.9799	0.897	0.9854
	308	43	0.0219	0.9290	0.83−0.98	1.106	0.843	0.9405	0.822	0.9855
	318	37	0.0269	0.9825	0.80−0.98	1.083	0.853	0.9881	0.822	0.9946
XAD761	288	93	0.0234	0.9985	0.82−0.98	2.269	0.896	0.9984	1.866	0.9980
	298	75	0.0282	0.9980	0.80−0.97	2.236	0.877	0.9980	1.773	0.9972
	308	104	0.0185	0.9961	0.86−0.98	2.037	0.906	0.9972	1.707	0.9981
	318	204	0.0076	0.9909	0.94−0.99	1.523	0.981	0.9902	1.470	0.9976

practical applications of XAD761 resin in the efficient recovery of 5-HMF from solution or actual hydrolysate.

3.3. Thermodynamics of 5-HMF Adsorption. The thermodynamics investigation, including Gibbs free energy change (ΔG), enthalpy change (ΔH), and entropy change (ΔS), provides important information to assess the nature and feasibility of the adsorption process, which were calculated by the following equations[62]

$$K_C = \frac{q_e}{C_e} \times \rho \tag{7}$$

$$\Delta G = -RT \ln K_C \tag{8}$$

$$\ln K_C = \frac{\Delta S}{R} - \frac{\Delta H}{RT} \tag{9}$$

https://doi.org/10.1021/acsomega.1c01894
ACS Omega 2021, 6, 16955−16968

Table 6. Isotherm Parameters of Each Isotherm Model for the Adsorption of Glucose onto Three Resins (XAD-4, XAD7HP, and XAD761)

		Langmuir				Freundlich			Henry	
resin	T (K)	q_m (mg/g)	K_L (L/g)	R^2	R_L	K_F (mg/g·(L/g)$^{1/n}$)	$1/n$	R^2	K_H (L/kg)	R^2
XAD-4	288	5507	1.325×10^{-4}	0.9555	1	0.599	1.100	0.9608	0.729	0.9871
	298	7015	9.355×10^{-5}	0.9782	1	0.511	1.127	0.9863	0.656	0.9937
	308	4605	1.313×10^{-4}	0.9807	1	0.519	1.078	0.9840	0.604	0.9947
	318	4937	1.006×10^{-4}	0.9728	1	0.390	1.122	0.9803	0.496	0.9919
XAD7HP	288	7031	9.869×10^{-5}	0.9898	1	0.566	1.104	0.9954	0.693	0.9972
	298	2122	3.102×10^{-4}	0.9788	1	0.586	1.058	0.9808	0.657	0.9942
	308	4798	1.173×10^{-4}	0.9564	1	0.435	1.131	0.9650	0.562	0.9866
	318	6228	7.954×10^{-5}	0.9683	1	0.363	1.158	0.9801	0.495	0.9902
XAD761	288	8015	3.024×10^{-5}	0.9343	1	0.104	1.426	0.9918	0.242	0.9772
	298	3232	6.151×10^{-5}	0.9626	1	0.140	1.177	0.9762	0.199	0.9892
	308	6504	2.712×10^{-5}	0.9317	1	0.074	1.435	0.9919	0.176	0.9763
	318	7028	2.142×10^{-5}	0.8997	1	0.049	1.567	0.9865	0.151	0.9613

Table 7. Comparison of the Maximum Sorption Capacity of XAD761 Resin for 5-HMF Adsorption with other Adsorption Resins

adsorption resin	temperature (K)	sorbent dose	maximum adsorption capacity	adsorption selectivity	references
SY-01	298	0.5−5.0 g/L (single-component solution)	107.73 mg/g		33
HCP	293	0.05 g/g_{sol}		>99%	32
Dowex Optipore L493	298	0.6 g/L (three-component solution)		>95%	60
PCL-PDE	288	4.985 g/L (single-component solution)	60.28 mg/g		41
HQ-18	298	0.61 g/L (multicomponent solution)		9.65 (selectivity coefficient)	61
XAD-4	288	0.51−5.06 g/L (single-component solution)	47 mg/g		this work
XAD7HP	288	0.51−5.06 g/L (single-component solution)	33 mg/g		this work
XAD761	288	0.51−5.06 g/L (single-component solution)	106 mg/g		this work

The thermodynamic parameters of 5-HMF adsorption onto the three resins are listed in Table 8. Clearly, negative values of ΔH and ΔG during the adsorption process at different temperatures indicated the exothermic and spontaneous adsorption process of 5-HMF onto the three resins. Moreover, the values of ΔH and ΔG were all less than 20 kJ mol^{-1}, indicating that the physical sorption governed the interaction between 5-HMF and XAD761 resin.[63] Under the same initial concentration of 5-HMF, the ΔH and ΔG absolute values of 5-HMF onto XAD761 resin were higher than those onto XAD-4 and XAD7HP resins, further suggesting that XAD761 resin possesses the best adsorption capacity to 5-HMF. These findings were consistent with the results of the adsorption isotherm.

Interestingly, the entropy changes of 5-HMF with various initial concentrations onto XAD761 resin were different. When the initial 5-HMF concentration is low, the adsorption of 5-HMF is an entropy decreasing process. Nevertheless, when the concentration increases to 3.08 g L^{-1}, the adsorption of 5-HMF is an entropy increasing process. This phenomenon may be due to the fact that the liquid phase adsorption process includes not only the adsorption of the adsorbate but also the desorption of the solvent (H_2O molecules).[64] When the initial concentration of 5-HMF is low, because the adsorption active sites are sufficient, the 5-HMF molecule is adsorbed by XAD761 resin, which is an orderly process with less confusion and entropy reduction.[65] When the initial 5-HMF concentration increases, more active sites are needed. The adsorption of 5-HMF must be accompanied by desorption of the same volume of solvent H_2O molecules. However, the molecular volume of 5-HMF is much larger than that of water molecules. In other words, the adsorption of one 5-HMF molecule will cause desorption of multiple H_2O molecules. Therefore, the entropy reduced by the adsorption of a 5-HMF molecule to the XAD761 resin is less than the entropy increased by desorption of several H_2O molecules from the resin, and the values of ΔS are greater than 0 at the high initial 5-HMF concentration system. The entropy increase may be regarded as the increase of disorder and randomness at the solution/solid interface caused by the desorption of H_2O molecules.[66]

3.4. Kinetic Studies. *3.4.1. Effect of Contact Time and Solution Temperature.* The contact time and solution temperature are essential parameters to establish an ideal chromatographic adsorption process.[67] The effect of solution temperature on the adsorption rate and adsorbed amount of 5-HMF onto XAD761 resin was investigated using an initial 5-HMF concentration of 2.71 g L^{-1} at 288, 298, 308, and 318 K and a fixed resin dosage for m = 20 g L^{-1} at a contact time t = 240 min (Figure 6, data given in Table S15). It is apparent that the adsorption rate of 5-HMF onto XAD761 resin increased significantly at the first stages of the contact period at all experiment temperatures, and then it decreased slowly near the equilibrium. It may be attributed to the fact that a great deal of adsorption sites on the XAD761 resin surface is sufficient for adsorption during the initial stage of the adsorption process, improving the rate of diffusion of the 5-HMF molecules across the external boundary layer.[68] With the extension of adsorption time, the available vacancy on the surface of XAD761 resin decreased gradually, and 5-HMF diffuses from the surface to the inside of the particle along the direction of the pore, which slowed down the adsorption rate until the adsorption reaches equilibrium. Besides, the equilibrium time of 5-HMF onto

https://doi.org/10.1021/acsomega.1c01894
ACS Omega 2021, 6, 16955−16968

Table 8. Thermodynamic Parameters for the Adsorption of 5-HMF onto Three Resins at Various Temperatures

		XAD-4			XAD7HP			XAD761		
C (g/L)	T (K)	ΔG (kJ mol^{-1})	ΔH (kJ mol^{-1})	ΔS (J mol^{-1} K^{-1})	ΔG (kJ mol^{-1})	ΔH (kJ mol^{-1})	ΔS (J mol^{-1} K^{-1})	ΔG (kJ mol^{-1})	ΔH (kJ mol^{-1})	ΔS (J mol^{-1} K^{-1})
0.51	288	−6.89	−12.31	−18.72	−5.11	−7.72	−8.95	−13.23	−26.32	−45.13
	298	−6.82			−5.20			−13.16		
	308	−6.44			−4.78			−12.15		
	318	−6.39			−4.95			−12.06		
1.04	288	−6.25	−9.42	−11.28	−4.72	−6.75	−7.22	−11.49	−15.79	−14.93
	298	−5.99			−4.57			−11.39		
	308	−5.85			−4.42			−11.07		
	318	−5.93			−4.54			−11.10		
1.52	288	−5.83	−9.79	−13.49	−4.49	−4.67	−0.76	−10.80	−13.89	−10.34
	298	−5.86			−4.47			−10.97		
	308	−5.68			−4.24			−11.49		
	318	−5.43			−4.56			−10.52		
2.04	288	−5.60	−8.23	−9.32	−4.36	−7.73	−11.91	−10.16	−13.57	−11.52
	298	−5.42			−4.11			−10.32		
	308	−5.26			−4.03			−9.91		
	318	−5.36			−4.00			−9.90		
2.56	288	−5.22	−5.68	−1.70	−3.79	−3.05	2.69	−9.67	−11.02	−4.52
	298	−5.09			−3.90			−9.72		
	308	−5.24			−3.88			−9.68		
	318	−5.12			−3.88			−9.52		
3.08	288	−5.15	−6.32	−4.24	−3.73	−2.87	2.87	−9.27	−9.26	0.16
	298	−4.99			−3.67			−9.36		
	308	−4.99			−3.78			−9.29		
	318	−5.01			−3.79			−9.30		
4.04	288	−4.85	−5.93	−4.00	−3.63	−1.11	7.65	−8.57	−8.08	1.97
	298	−4.63			−3.39			−8.74		
	308	−4.68			−3.45			−8.79		
	318	−4.71			−3.54			−8.61		
5.06	288	−4.50	−5.36	−3.02	−3.25	−2.53	2.39	−8.13	−6.29	6.44
	298	−4.45			−3.24			−8.21		
	308	−4.44			−3.21			−8.30		
	318	−4.40			−3.34			−8.31		

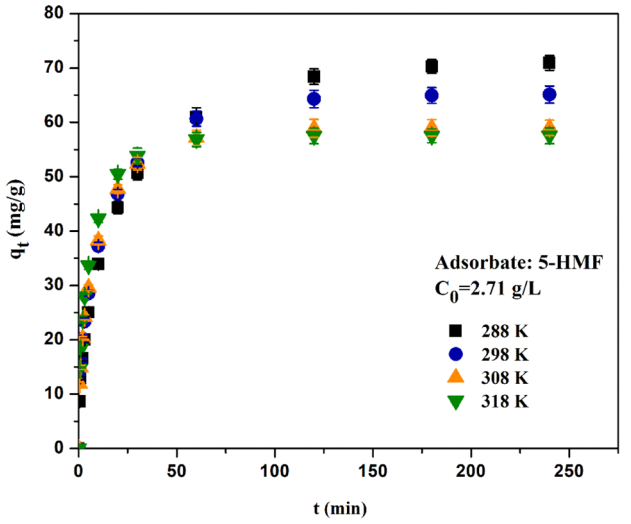

Figure 6. Effect of temperature on the adsorption rate of 5-HMF adsorbed onto XAD761 resin at initial concentration C_0 = 2.71 g L^{-1} and resin dosage m = 20 g L^{-1}.

XAD761 resin was found to decrease from 120 to 60 min with the increasing solution temperature from 288 to 318 K, revealing that the higher temperature is beneficial to accelerate the diffusion rate of 5-HMF onto XAD761 resin and shorten the time required for adsorption equilibrium. However, increasing the temperature also reduces the equilibrium adsorption capacity. The equilibrium adsorption capacity of 288 K was the highest among the studied temperatures, further suggesting the exothermic nature of the adsorption process. This result was consistent with the adsorption equilibrium results and the adsorption thermodynamic analysis discussed above.

3.4.2. Adsorption Kinetics. Detailed adsorption kinetic model studies are useful to understand the mass transfer mechanism and law of adsorbate onto adsorbents.[69] In this work, the Lagergren's pseudo-first-order,[70] Mckay pseudo-second-order,[71] and Weber−Morris intraparticle diffusion model[72] were applied to describe the adsorption kinetics.

$$\text{Lagergren's pseudo first-order } \ln(q_e - q_t) = \ln q_e - k_1 t \quad (10)$$

$$\text{Mckay pseudo second-order } \frac{t}{q_t} = \frac{1}{k_2 q_e^{\,2}} + \frac{t}{q_e} \quad (11)$$

$$\text{Weber−Morris intraparticle diffusion model } q_t = k_i t^{1/2} + C \quad (12)$$

https://doi.org/10.1021/acsomega.1c01894
ACS Omega 2021, 6, 16955−16968

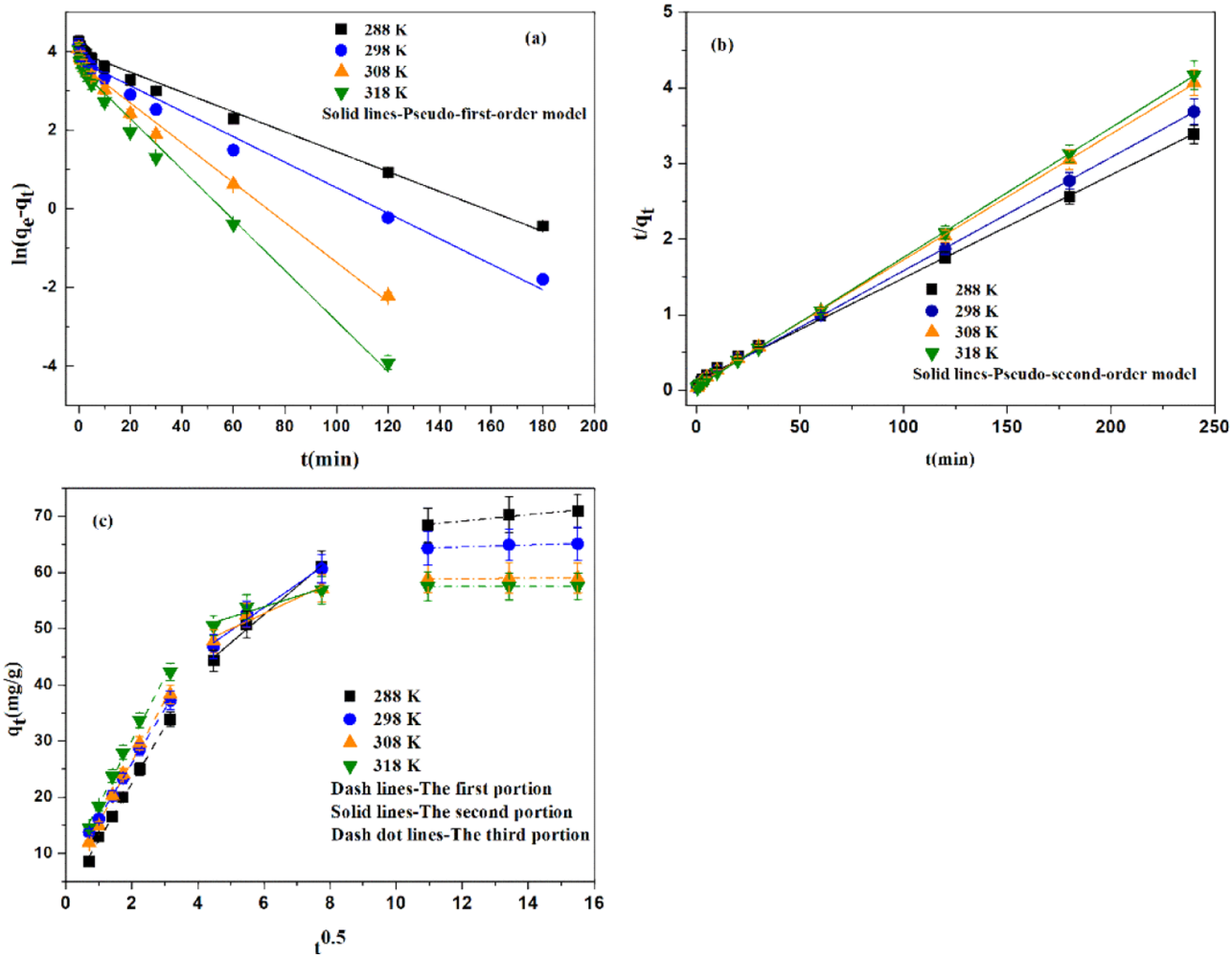

Figure 7. Pseudo-first-order (a), pseudo-second-order (b), and intraparticle diffusion (c) kinetic models for the adsorption of 5-HMF onto XAD761 resin at various temperatures.

Table 9. Kinetic Parameters for the Adsorption of 5-HMF Onto XAD761 Resin at Various Temperatures (C_o = 2.71 g L^{-1})

		pseudo first-order			pseudo second-order					intraparticle diffusion			
T	q_{exp} (mg/g)	q_{cal} (mg/g)	k_1 (min^{-1})	R^2	q_{cal} (mg/g)	k_2 (g mg^{-1} min^{-1})	R^2	$k_{i,1}$ (mg g^{-1} $h^{1/2}$)	R^2	$k_{i,2}$ (mg g^{-1} $h^{1/2}$)	R^2	$k_{i,3}$ (mg g^{-1} $h^{1/2}$)	R^2
288	70.9	53.8	0.0253	0.9887	73.7	0.0015	0.9984	10.103	0.9965	4.999	0.9851	0.561	0.9009
298	65.1	43.9	0.0324	0.9855	66.8	0.0026	0.9993	9.678	0.9994	4.106	0.9695	0.179	0.8513
308	59.0	40.8	0.0507	0.9885	60.2	0.0041	0.9998	10.890	0.9944	2.733	0.9126	0.025	0.5716
318	57.5	36.0	0.0644	0.9887	58.3	0.0064	0.9999	11.361	0.9916	1.846	0.8736	0.004	0.9656

Figure 7 (data given in Tables S16–S18) shows the adsorption kinetics of 5-HMF onto XAD761 resin at various temperatures, which were analyzed by the measurement of time-dependent adsorption capacities. The corresponding kinetic parameters are listed in Table 9. It is apparent from Figure 7B and Table 9 that the pseudo-second-order model presented linear correlation, and the R^2 values was very close to 1 and higher than those of the pseudo-first-order model (see Figure 7A). Furthermore, the values of q_{cal} calculated using the pseudo-second-order model also agreed with the experimental results, q_{exp} (see Table 9). It is worth noting that the model parameter k_2 increased with the increasing solution temperature from 288 to 318 K, resulting from the low viscosity and rapid diffusion of 5-HMF molecules in solution at high temperature and leading to the accelerated adsorption rate of 5-HMF onto XAD761 resin.[73]

In addition, Figure 7c presents the adsorption process of 5-HMF onto XAD 761 resin divided into three linear curves without passing through the origin, suggesting that intraparticle diffusion is not the only rate-limiting step. The first stage (0–10 min) was considered to be the diffusion of 5-HMF from the bulk solution to the boundary layer film of the solvent and transport from the film of the solvent onto the external surface of XD761 resin, which was controlled by film diffusion. At the second stage (20–60 min), 5-HMF entered into XAD761 resin particle pores from resin particle surface through intraparticle diffusion. Then, at the third stage, the adsorption reached saturation state finally because most 5-HMF molecules was adsorbed by XAD761 resin and the low 5-HMF concentration remained in the solution. Furthermore, the diffusion rate parameters of mass transfer at different stages are given in Table 9. It can be seen that the values of $k_{i,1}$ and

https://doi.org/10.1021/acsomega.1c01894
ACS Omega 2021, 6, 16955–16968

$k_{i,2}$ were much higher than $k_{i,3}$, illustrating that the equilibrium stage is quite fast.[65]

3.4.3. Adsorption Activation Energy. The activation energy (E_a) for the adsorption of 5-HMF onto XAD761 resin was calculated by the Arrhenius equation[74]

$$\ln k_2 = \ln A - \frac{E_a}{RT} \quad (13)$$

The values of A and E_a were calculated from the intercept and slope of the plotted line ln k_2 versus $1/T$ (see Figure 8, data given in Table S19), respectively. In the current study, the activation energy calculated by Arrhenius equation was 36.64 kJ mol^{-1}, indicating that physical sorption plays an important role in the adsorption of 5-HMF on XAD761 resin.[75] The results of activation energy analysis are consistent with those of thermodynamic analysis in Section 3.3. Moreover, the positive value of E_a suggested that the adsorption rate would increase with increasing solution temperature, which is in accordance with the values of the rate constants (see Table 9).

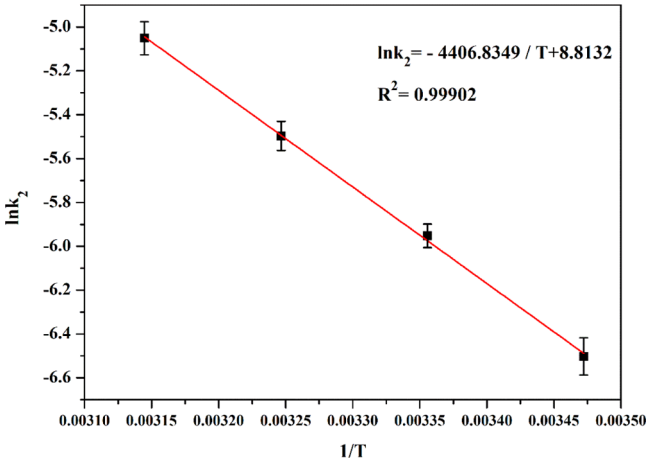

Figure 8. Plot of Arrhenius equation for the adsorption of 5-HMF onto XAD761 resin.

4. CONCLUSIONS

In this study, various porous polymers (XAD-4, XAD7HP, and XAD761 resin) modified by different functional groups were used to adsorb 5-HMF, LA, FA, and glucose from aqueous solutions. Experimental results showed that XAD761 resin possessed the highest 5-HMF selectivity and uptake for 5-HMF. During the experimental concentration range (0.51−5.06 g L^{-1}) at 288 K, the maximum capacity of 5-HMF onto XAD761 resin reached 106 mg g^{-1} wet resin. Moreover, the Freundlich isotherm model could well fit the equilibrium data of 5-HMF at various temperatures. The thermodynamic results revealed that the adsorption process of 5-HMF on XAD761 resin was a spontaneous and exothermic process. Furthermore, the kinetic data of 5-HMF onto XAD761 resin was followed by the pseudo-second-order kinetic model. The activation energy was 36.64 kJ mol^{-1}, implying that the adsorption process was physical adsorption. Accordingly, the phenol hydroxyl group-modified XAD761 resin showed an excellent adsorption performance to 5-HMF, which not only provides a new choice for the separation and purification of 5-HMF from aqueous solution or real hydrolysates but also provides a new direction for the development of resin synthesis technology.

■ ASSOCIATED CONTENT

Supporting Information

The Supporting Information is available free of charge at https://pubs.acs.org/doi/10.1021/acsomega.1c01894.

Adsorption capacity of 5-HMF (5.021 g L^{-1}), LA (20.251 g L^{-1}), FA (9.103 g L^{-1}), and glucose (9.854 g L^{-1}) onto XAD-4, XAD7HP, and XAD761 resins in a multicomponent system at 298 ± 1 K; adsorption selectivity of 5-HMF (5.021 g L^{-1}), LA (20.251 g L^{-1}), FA (9.103 g L^{-1}), and glucose (9.854 g L^{-1}) onto XAD-4, XAD7HP and XAD761 resins in a multicomponent system at 298 ± 1 K; 5-HMF adsorption capacity on XAD-4 resin in a single-component system at various temperatures; 5-HMF adsorption capacity on XAD7HP resin in a single-component system at various temperatures; 5-HMF adsorption capacity on XAD761 resin in a single-component system at various temperatures; LA adsorption capacity on XAD-4 resin in a single-component system at various temperatures; LA adsorption capacity on XAD7HP resin in a single-component system at various temperatures; LA adsorption capacity on XAD761 resin in a single-component system at various temperatures; FA adsorption capacity on XAD-4 resin in a single-component system at various temperatures; FA adsorption capacity on XAD7HP resin in a single-component system at various temperatures; FA adsorption capacity on XAD761 resin in a single-component system at various temperatures; glucose adsorption capacity on XAD-4 resin in a single-component system at various temperatures; glucose adsorption capacity on XAD7HP resin in a single-component system at various temperatures; glucose adsorption capacity on XAD761 resin in a single-component system at various temperatures; effect of temperature on the adsorption rate of 5-HMF adsorbed onto XAD761 resin at initial concentration C_0 = 2.71 g L^{-1} and resin dosage m = 20 g L^{-1}; pseudo-first-order kinetic models for the adsorption of 5-HMF onto XAD761 resin at various temperatures; pseudo-second-order kinetic models for the adsorption of 5-HMF onto XAD761 resin at various temperatures; intraparticle diffusion kinetic models for the adsorption of 5-HMF onto XAD761 resin at various temperatures; and plot of Arrhenius equation for the adsorption of 5-HMF onto XAD761 resin (PDF)

■ AUTHOR INFORMATION

Corresponding Author

Xiaoqing Lin − *School of Chemical Engineering and Light Industry, Guangdong University of Technology, Guangzhou 510006, People's Republic of China; Guangdong Key Laboratory of Plant Resources Biorefinery and Guangzhou Key Laboratory of Clean Transportation Energy Chemistry, Guangdong University of Technology, Guangzhou 510006, People's Republic of China;* orcid.org/0000-0002-1751-5348; Email: linxiaoqing@gdut.edu.cn

Authors

Lei Hu − *School of Chemical Engineering and Light Industry, Guangdong University of Technology, Guangzhou 510006, People's Republic of China*

Jiayi Zheng − *School of Chemical Engineering and Light Industry, Guangdong University of Technology, Guangzhou 510006, People's Republic of China*
Qing Li − *School of Chemical Engineering and Light Industry, Guangdong University of Technology, Guangzhou 510006, People's Republic of China*
Shunhui Tao − *School of Chemical Engineering and Light Industry, Guangdong University of Technology, Guangzhou 510006, People's Republic of China*
Xiaojie Zheng − *School of Chemical Engineering and Light Industry, Guangdong University of Technology, Guangzhou 510006, People's Republic of China*
Xiaodong Zhang − *School of Chemical Engineering and Light Industry, Guangdong University of Technology, Guangzhou 510006, People's Republic of China*
Yao Liu − *School of Chemical Engineering and Light Industry, Guangdong University of Technology, Guangzhou 510006, People's Republic of China*

Complete contact information is available at: https://pubs.acs.org/10.1021/acsomega.1c01894

Author Contributions

[‖]L.H. and J.Z. contributed equally to this study.

Notes

The authors declare no competing financial interest.

■ ACKNOWLEDGMENTS

This work was supported by the financial support of the National Natural Science Foundation of China (21978053, 51508547), the Project of Pearl River S&T Nova Program of Guangzhou (201710010096), the Key Area R&D Program of Guangdong Province (2020B0101070001), and the "One-Hundred Young Talents" Program of Guangdong University of Technology (220413185).

■ NOTATION

A	Arrhenius constant
C_0	initial concentration (g L^{-1})
C_e	equilibrium concentration (g L^{-1})
C_t	concentration at contact time (g L^{-1})
K_L	Langmuir adsorption isotherm constant (L g^{-1})
K_F	Freundlich adsorption isotherm constant (mg g^{-1})(L $g^{-1})^{1/n}$
K_H	Henry adsorption isotherm constant (L kg^{-1})
K_c	thermodynamic equilibrium constant
R_L	separation factor
m	mass of the wet resin (g)
n	Freundlich adsorption isotherm constant
q_e	equilibrium adsorption capacity (mg g^{-1})
$q_{e,cal}$	calculate adsorption capacity (mg g^{-1})
$q_{e,exp}$	experimental adsorption capacity (mg g^{-1})
q_m	maximum saturated adsorption capacity (mg g^{-1})
q_t	adsorption capacity at contact time (mg g^{-1})
R	gas constant (8.314 J mol^{-1} K^{-1})
T	solution temperature (K)
t	contact time (min)
V	volume of solution (mL)
ΔG	Gibbs free energy change (kJ mol^{-1})
ΔH	enthalpy change (kJ mol^{-1})
ΔS	entropy change (J mol^{-1} K^{-1})
α	selectivity factor
E_a	apparent activation energy (kJ mol^{-1})
k_1	pseudo-first-order rate constant (min^{-1})
k_2	pseudo-second-order rate constant (mg g^{-1} min^{-1})
k_i	intraparticle diffusion rate constant (mg g^{-1} $min^{-1/2}$)
ρ	the density of the solution (g L^{-1})

■ REFERENCES

(1) Hu, L.; Jiang, Y.; Wu, Z.; Wang, X.; He, A.; Xu, J.; Xu, J. State-of-the-art advances and perspectives in the separation of biomass-derived 5-hydroxymethylfurfural. *J. Cleaner Prod.* **2020**, *276*, 124219.
(2) Gérardy, R.; Debecker, D. P.; Estager, J.; Luis, P.; Monbaliu, J.-C. M. Continuous Flow Upgrading of Selected C2−C6 Platform Chemicals Derived from Biomass. *Chem. Rev.* **2020**, *120*, 7219−7347.
(3) Ragauskas, A. J.; Williams, C. K.; Davison, B. H.; Britovsek, G.; Cairney, J.; Eckert, C. A.; Frederick, W. J.; Hallett, J. P.; Leak, D. J.; Liotta, C. L. The path forward for biofuels and biomaterials. *Science* **2006**, *311*, 484−489.
(4) Corma, A.; Iborra, S.; Velty, A. Chemical Routes for the Transformation of Biomass into Chemicals. *Chem. Rev.* **2007**, *107*, 2411−2502.
(5) Li, X.; Xu, R.; Yang, J.; Nie, S.; Liu, D.; Liu, Y.; Si, C. Production of 5-hydroxymethylfurfural and levulinic acid from lignocellulosic biomass and catalytic upgradation. *Ind. Crop. Prod.* **2019**, *130*, 184−197.
(6) Lin, X.; Liu, Y.; Zheng, X.; Qureshi, N. High-efficient cellulosic butanol production from deep eutectic solvent pretreated corn stover without detoxification. *Ind. Crop. Prod.* **2021**, *162*, 113258.
(7) Overton, J. C.; Engelberth, A. S.; Mosier, N. S. Single-Vessel Synthesis of 5-Hydroxymethylfurfural (HMF) from Milled Corn. *ACS Sustainable Chem. Eng.* **2020**, *8*, 18−21.
(8) Thoma, C.; Konnerth, J.; Sailer-Kronlachner, W.; Solt, P.; Rosenau, T.; Herwijnen, H. W. G. Current Situation of the Challenging Scale-Up Development of Hydroxymethylfurfural Production. *ChemSusChem* **2020**, *13*, 3544−3564.
(9) van Putten, R.-J.; van der Waal, J. C.; de Jong, E.; Rasrendra, C. B.; Heeres, H. J.; de Vries, J. G. Hydroxymethylfurfural A Versatile Platform Chemical Made from Renewable Resources. *Chem. Rev.* **2013**, *113*, 1499−1597.
(10) Zhao, H.; Holladay, J. E.; Brown, H.; Zhang, Z. C. Metal chlorides in ionic liquid solvents convert sugars to 5-hydroxymethylfurfural. *Science* **2007**, *316*, 1597−1600.
(11) Roman-Leshkov, Y.; Chheda, J. N.; Dumesic, J. A. Phase modifiers promote efficient production of hydroxymethylfurfural from fructose. *Science* **2006**, *312*, 1933−1937.
(12) Yan, P.; Xia, M.; Chen, S.; Han, W.; Wang, H.; Zhu, W. Unlocking biomass energy: continuous high-yield production of 5-hydroxymethylfurfural in water. *Green Chem.* **2020**, *22*, 5274−5284.
(13) Hou, Q.; Qi, X.; Zhen, M.; Qian, H.; Nie, Y.; Bai, C.; Zhang, S.; Bai, X.; Ju, M. Biorefinery roadmap based on catalytic production and upgrading 5-hydroxymethylfurfural. *Green Chem.* **2021**, *23*, 119−231.
(14) Ban, H.; Pan, T.; Cheng, Y.; Wang, L.; Li, X. Solubilities of 2,5-Furandicarboxylic Acid in Binary Acetic Acid + Water, Methanol + Water, and Ethanol + Water Solvent Mixtures. *J. Chem. Eng. Data* **2018**, *63*, 1987−1993.
(15) Muranaka, Y.; Nakagawa, H.; Masaki, R.; Maki, T.; Mae, K. Continuous 5-Hydroxymethylfurfural Production from Monosaccharides in a Microreactor. *Ind. Eng. Chem. Res.* **2017**, *56*, 10998−11005.
(16) Chen, S.; Wojcieszak, R.; Dumeignil, F.; Marceau, E.; Royer, S. How Catalysts and experimental conditions determine the selective hydroconversion of furfural and 5-hydroxymethylfurfural. *Chem. Rev.* **2018**, *118*, 11023−11117.
(17) Wu, Q.; Zhang, G.; Gao, M.; Cao, S.; Li, L.; Liu, S.; Xie, C.; Huang, L.; Yu, S.; Ragauskas, A. J. Clean production of 5-hydroxymethylfurfural from cellulose using a hydrothermal/biomass-based carbon catalyst. *J. Cleaner Prod.* **2019**, *213*, 1096−1102.
(18) Hayashi, E.; Yamaguchi, Y.; Kamata, K.; Tsunoda, N.; Kumagai, Y.; Oba, F.; Hara, M. Effect of MnO2 Crystal Structure on Aerobic Oxidation of 5-Hydroxymethylfurfural to 2,5-Furandicarboxylic Acid. *J. Am. Chem. Soc.* **2019**, *141*, 890−900.

(19) Song, X.; Liu, X.; Wang, H.; Guo, Y.; Wang, Y. Improved Performance of Nickel Boride by Phosphorus Doping as an Efficient Electrocatalyst for the Oxidation of 5-Hydroxymethylfurfural to 2,5-Furandicarboxylic Acid. *Ind. Eng. Chem. Res.* **2020**, *59*, 17348−17356.
(20) Xu, J. J.; Su, T.; Zhu, Z. G.; Chen, N. M.; Hao, D. M.; Wang, M. R.; Zhao, Y. C.; Ren, W. Z.; Lu, H. Y. Biomimetic oxygen activation and electron transfer for aerobic oxidative 5-hydroxymethylfurfural to 2,5-diformylfuran. *Chem. Eng. J.* **2020**, *396*, 125303.
(21) Sajid, M.; Zhao, X.; Liu, D. Production of 2,5-furandicarboxylic acid (FDCA) from 5-hydroxymethylfurfural (HMF): recent progress focusing on the chemical-catalytic routes. *Green Chem.* **2018**, *20*, 5427−5453.
(22) Asghari, F. S.; Yoshida, H. Kinetics of the decomposition of fructose catalyzed by hydrochloric acid in subcritical water: Formation of 5-hydroxymethylfurfural, levulinic, and formic acids. *Ind. Eng. Chem. Res.* **2007**, *46*, 7703−7710.
(23) Jin, C.; Yang, M.; E, S.; Liu, J.; Zhang, S.; Zhang, X.; Sheng, K.; Zhang, X. Corn stover valorization by one-step formic acid fractionation and formylation for 5-hydroxymethylfurfural and high guaiacyl lignin production. *Bioresour. Technol.* **2020**, *299*, 122586.
(24) Sayed, M.; Warlin, N.; Hulteberg, C.; Munslow, I.; Lundmark, S.; Pajalic, O.; Tunå, P.; Zhang, B.; Pyo, S.-H.; Hatti-Kaul, R. 5-Hydroxymethylfurfural from fructose: an efficient continuous process in a water-dimethyl carbonate biphasic system with high yield product recovery. *Green Chem.* **2020**, *22*, 5402−5413.
(25) Jeong, G.-T.; Kim, S.-K. Statistical optimization of levulinic acid and formic acid production from lipid-extracted residue of Chlorella vulgaris. *J. Environ. Chem. Eng.* **2021**, *9*, 105142.
(26) Zhang, Y.-B.; Luo, Q.-X.; Lu, M.-H.; Luo, D.; Liu, Z.-W.; Liu, Z.-T. Controllable and scalable synthesis of hollow-structured porous aromatic polymer for selective adsorption and separation of HMF from reaction mixture of fructose dehydration. *Chem. Eng. J.* **2019**, *358*, 467−479.
(27) Yong, G.; Zhang, Y.; Ying, J. Y. Efficient catalytic system for the selective production of 5-hydroxymethylfurfural from glucose and fructose. *Angew. Chem., Int. Ed.* **2008**, *47*, 9345−9348.
(28) Babaei, Z.; Najafi Chermahini, A.; Dinari, M.; Saraji, M.; Shahvar, A. Cleaner production of 5-hydroxymethylfurfural from fructose using ultrasonic propagation. *J. Cleaner Prod.* **2018**, *198*, 381−388.
(29) Shi, C.; Xin, J.; Liu, X.; Lu, X.; Zhang, S. Using sub/supercritical CO_2 as "phase separation switch" for the efficient production of 5-hydroxymethylfurfural from fructose in an ionic liquid/organic biphasic system. *ACS Sustainable Chem. Eng.* **2015**, *4*, 557−563.
(30) Vinke, P.; Van Bekkum, H. The dehydration of fructose towards 5-hydroxymethylfurfural using activated carbon as adsorbent. *Starch/Staerke* **1992**, *44*, 90−96.
(31) Ranjan, R.; Thust, S.; Gounaris, C. E.; Woo, M.; Floudas, C. A.; Keitz, M. v.; Valentas, K. J.; Wei, J.; Tsapatsis, M. Adsorption of fermentation inhibitors from lignocellulosic biomass hydrolyzates for improved ethanol yield and value-added product recovery. *Microporous Mesoporous Mater.* **2009**, *122*, 143−148.
(32) Detoni, C.; Gierlich, C. H.; Rose, M.; Palkovits, R. Selective Liquid Phase Adsorption of 5-Hydroxymethylfurfural on Nanoporous Hyper-Cross-Linked Polymers. *ACS Sustainable Chem. Eng.* **2014**, *2*, 2407−2415.
(33) Zheng, J.; Pan, B.; Xiao, J.; He, X.; Chen, Z.; Huang, Q.; Lin, X. Experimental and Mathematical Simulation of Noncompetitive and Competitive Adsorption Dynamic of Formic Acid−Levulinic Acid−5-Hydroxymethylfurfural from Single, Binary, and Ternary Systems in a Fixed-Bed Column of SY-01 Resin. *Ind. Eng. Chem. Res.* **2018**, *57*, 8518−8528.
(34) León, M.; Swift, T. D.; Nikolakis, V.; Vlachos, D. G. Adsorption of the compounds encountered in monosaccharide dehydration in zeolite beta. *Langmuir* **2013**, *29*, 6597−6605.
(35) Zheng, J.; Hu, L.; He, X.; Liu, Y.; Zheng, X.; Tao, S.; Lin, X. Evaluation of Pore Structure of Polarity-Controllable Post-Cross-Linked Adsorption Resins on the Adsorption Performance of 5-Hydroxymethylfurfural in Both Single- and Ternary-Component Systems. *Ind. Eng. Chem. Res.* **2020**, *59*, 17575−17586.
(36) Zhao, Y.; Xu, J.; Wang, J.; Wu, J.; Gao, M.; Zheng, B.; Xu, H.; Shi, Q.; Dong, J. Adsorptive Separation of Furfural/5-Hydroxymethylfurfural in MAF-5 with Ellipsoidal Pores. *Ind. Eng. Chem. Res.* **2020**, *59*, 11734−11742.
(37) Altway, S.; Pujar, S. C.; de Haan, A. B. Liquid-liquid equilibria of ternary and quaternary systems involving 5-hydroxymethylfurfural, water, organic solvents, and salts at 313.15 K and atmospheric pressure. *Fluid Phase Equilib.* **2018**, *475*, 100−110.
(38) Ijzer, A. C.; Vriezekolk, E.; Đekic Zivkovic, T.; Nijmeijer, K. Adsorption kinetics of Dowex(TM) Optipore(TM) L493 for the removal of the furan 5-hydroxymethylfurfural from sugar. *J. Chem. Technol. Biotechnol.* **2016**, *91*, 96−104.
(39) IJzer, A. C.; Vriezekolk, E.; Rolevink, E.; Nijmeijer, K. Performance analysis of aromatic adsorptive resins for the effective removal of furan derivatives from glucose. *J. Chem. Technol. Biotechnol.* **2015**, *90*, 101−109.
(40) Li, L.; Yang, L.; Wang, J.; Zhang, Z.; Yang, Q.; Yang, Y.; Ren, Q.; Bao, Z. Highly efficient separation of methane from nitrogen on a squarate-based metal-organic framework. *AIChE J.* **2018**, *64*, 3681−3689.
(41) Zheng, J.; He, X.; Cai, C.; Xiao, J.; Liu, Y.; Chen, Z.; Pan, B.; Lin, X. Adsorption isotherm, kinetics simulation and breakthrough analysis of 5-hydroxymethylfurfural adsorption/desorption behavior of a novel polar-modified post-cross-linked poly (divinylbenzene-co-ethyleneglycoldimethacrylate) resin. *Chemosphere* **2020**, *239*, 124732.
(42) Lin, X.; Huang, Q.; Qi, G.; Xiong, L.; Huang, C.; Chen, X.; Li, H.; Chen, X. Adsorption behavior of levulinic acid onto microporous hyper-cross-linked polymers in aqueous solution: Equilibrium, thermodynamic, kinetic simulation and fixed-bed column studies. *Chemosphere* **2017**, *171*, 231−239.
(43) Lin, X.; Huang, Q.; Qi, G.; Shi, S.; Xiong, L.; Huang, C.; Chen, X.; Li, H.; Chen, X. Estimation of fixed-bed column parameters and mathematical modeling of breakthrough behaviors for adsorption of levulinic acid from aqueous solution using SY-01 resin. *Sep. Purif. Technol.* **2017**, *174*, 222−231.
(44) Gan, Y.; Chen, G.; Sang, Y.; Zhou, F.; Man, R.; Huang, J. Oxygen-rich hyper-cross-linked polymers with hierarchical porosity for aniline adsorption. *Chem. Eng. J.* **2019**, *368*, 29−36.
(45) Chen, Q.; Luo, M.; Hammershøj, P.; Zhou, D.; Han, Y.; Laursen, B. W.; Yan, C.-G.; Han, B.-H. Microporous polycarbazole with high specific surface area for gas storage and separation. *J. Am. Chem. Soc.* **2012**, *134*, 6084−6087.
(46) Shao, L.; Wang, S.; Liu, M.; Huang, J.; Liu, Y.-N. Triazine-based hyper-cross-linked polymers derived porous carbons for CO_2 capture. *Chem. Eng. J.* **2018**, *339*, 509−518.
(47) Zhang, C.; Zhu, P.-C.; Tan, L.; Liu, J.-M.; Tan, B.; Yang, X.-L.; Xu, H.-B. Triptycene-Based Hyper-Cross-Linked Polymer Sponge for Gas Storage and Water Treatment. *Macromolecules* **2015**, *48*, 8509−8514.
(48) Dong, K.; Zhang, J.; Luo, W.; Su, L.; Huang, Z. Catalytic conversion of carbohydrates into 5-hydroxymethyl furfural over sulfonated hyper-cross-linked polymer in DMSO. *Chem. Eng. J.* **2018**, *334*, 1055−1064.
(49) Pincus, L. N.; Petrović, P. V.; Gonzalez, I. S.; Stavitski, E.; Fishman, Z. S.; Rudel, H. E.; Anastas, P. T.; Zimmerman, J. B. Selective adsorption of arsenic over phosphate by transition metal cross-linked chitosan. *Chem. Eng. J.* **2021**, *412*, 128582.
(50) Nielsen, L.; Bandosz, T. J. Analysis of the competitive adsorption of pharmaceuticals on waste derived materials. *Chem. Eng. J.* **2016**, *287*, 139−147.
(51) Foo, K. Y.; Hameed, B. H. Insights into the modeling of adsorption isotherm systems. *Chem. Eng. J.* **2010**, *156*, 2−10.
(52) Uslu, H.; Datta, D.; Santos, D.; Öztürk, M. Separation of Levulinic Acid Using Polymeric Resin, Amberlite IRA-67. *J. Chem. Eng. Data* **2019**, *64*, 3044−3049.

https://doi.org/10.1021/acsomega.1c01894
ACS Omega 2021, 6, 16955−16968

(53) Langmuir, I. The constitution and fundamental properties of solids and liquids. Part I. Solids. *J. Am. Chem. Soc.* **1916**, *38*, 2221−2295.
(54) Freundlich, H. Über die adsorption in lösungen. *Z. Phys. Chem.* **1907**, *57*, 385−470.
(55) Al-Ghouti, M. A.; Da'ana, D. A. Guidelines for the use and interpretation of adsorption isotherm models: A review. *J. Hazard Mater.* **2020**, *393*, 122383.
(56) Weber, T. W.; Chakravorti, R. K. Pore and solid diffusion models for fixed-bed adsorbers. *AIChE J.* **1974**, *20*, 228−238.
(57) Zeidan, H.; Marti, M. E. Separation of Formic Acid from Aqueous Solutions onto Anion Exchange Resins: Equilibrium, Kinetic, and Thermodynamic Data. *J. Chem. Eng. Data* **2019**, *64*, 2718−2727.
(58) Jawad, A. H.; Abdulhameed, A. S. Mesoporous Iraqi red kaolin clay as an efficient adsorbent for methylene blue dye: Adsorption kinetic, isotherm and mechanism study. *Surf. Interfaces* **2020**, *18*, 100422.
(59) Buran, T. J.; Sandhu, A. K.; Li, Z.; Rock, C. R.; Yang, W. W.; Gu, L. Adsorption/desorption characteristics and separation of anthocyanins and polyphenols from blueberries using macroporous adsorbent resins. *J. Food Eng.* **2014**, *128*, 167−173.
(60) Lee, S. C. Removal and recovery of acetic acid and two furans during sugar purification of simulated phenols-free biomass hydrolysates. *Bioresour. Technol.* **2017**, *245*, 116−122.
(61) Huang, Q.; Zhang, H.; Xiong, L.; Huang, C.; Guo, H.; Chen, X.; Luo, M.; Tian, L.; Lin, X.; Chen, X. Controllable Synthesis of Styrene-divinylbenzene Adsorption Resins and the Effect of Textural Properties on Removal Performance of Fermentation Inhibitors from Rice Straw Hydrolysate. *Ind. Eng. Chem. Res.* **2018**, *57*, 5119−5127.
(62) Akram, M.; Bhatti, H. N.; Iqbal, M.; Noreen, S.; Sadaf, S. Biocomposite efficiency for Cr(VI) adsorption: Kinetic, equilibrium and thermodynamics studies. *J. Environ. Chem. Eng.* **2017**, *5*, 400−411.
(63) Eder, S.; Müller, K.; Azzari, P.; Arcifa, A.; Peydayesh, M.; Nyström, L. Mass Transfer Mechanism and Equilibrium Modelling of Hydroxytyrosol Adsorption on Olive Pit−Derived Activated Carbon. *Chem. Eng. J.* **2021**, *404*, 126519.
(64) Manes, M.; Hofer, L. J. E. Application of the Polanyi adsorption potential theory to adsorption from solution on activated carbon. *J. Phys. Chem.* **1969**, *73*, 584−590.
(65) Elmi, F.; Mohammadi Damghani, F.; Shokrollahzadeh Taleshi, M. Kinetic and Isotherm Studies of Adsorption of the Metribuzin Herbicide on an Fe3O4/CNT@PDA Hybrid Magnetic Nanocomposite in Wastewater. *Ind. Eng. Chem. Res.* **2020**, *59*, 9604−9610.
(66) Carvajal-Bernal, A. M.; Gómez-Granados, F.; Giraldo, L.; Moreno-Piraján, J. C.; Balsamo, M.; Erto, A. Kinetic and thermodynamic study of n-pentane adsorption on activated carbons modified by either carbonization or impregnation with ammonium hydroxide. *Microporous Mesoporous Mater.* **2020**, *302*, 110196.
(67) Lin, X.; Wu, J.; Fan, J.; Qian, W.; Zhou, X.; Qian, C.; Jin, X.; Wang, L.; Bai, J.; Ying, H. Adsorption of butanol from aqueous solution onto a new type of macroporous adsorption resin: studies of adsorption isotherms and kinetics simulation. *J. Chem. Technol. Biotechnol.* **2012**, *87*, 924−931.
(68) Tavlieva, M. P.; Genieva, S. D.; Georgieva, V. G.; Vlaev, L. T. Kinetic study of brilliant green adsorption from aqueous solution onto white rice husk ash. *J. Colloid Interface Sci.* **2013**, *409*, 112−122.
(69) Zhang, H.; Tong, Z.; Wei, T.; Tang, Y. Removal characteristics of Zn(II) from aqueous solution by alkaline Ca-bentonite. *Desalination* **2011**, *276*, 103−108.
(70) Lagergren, S. About the Theory of So-Called Adsorption of Soluble Substances. *K. Sven. Vetenskapsakad. Handl.* **1898**, *24*, 1−39.
(71) Ho, Y. S.; McKay, G. Kinetic Models for the Sorption of Dye from Aqueous Solution by Wood. *Process Saf. Environ.* **1998**, *76*, 183−191.
(72) Weber, W. J.; Morris, J. C. Kinetics of Adsorption on Carbon from Solution. *J. Sanit. Eng. Div.* **1963**, *89*, 31−59.
(73) Ahmad, A. L.; Chan, C. Y.; Abd Shukor, S. R.; Mashitah, M. D. Adsorption kinetics and thermodynamics of β-carotene on silica-based adsorbent. *Chem. Eng. J.* **2009**, *148*, 378−384.
(74) Monte Blanco, S. P. D.; Scheufele, F. B.; Módenes, A. N.; Espinoza-Quiñones, F. R.; Marin, P.; Kroumov, A. D.; Borba, C. E. Kinetic, equilibrium and thermodynamic phenomenological modeling of reactive dye adsorption onto polymeric adsorbent. *Chem. Eng. J.* **2017**, *307*, 466−475.
(75) Huang, Q.; Lin, X.; Xiong, L.; Huang, C.; Zhang, H.; Luo, M.; Tian, L.; Chen, X. Equilibrium, kinetic and thermodynamic studies of acid soluble lignin adsorption from rice straw hydrolysate by a self-synthesized macro/mesoporous resin. *RSC Adv.* **2017**, *7*, 23896−23906.

https://doi.org/10.1021/acsomega.1c01894
ACS Omega 2021, 6, 16955−16968